



OPEN

METALIC reveals interorganelle lipid flux in live cells by enzymatic mass tagging

Arun T. John Peter^{1,3}✉, Carmelina Petrunaro¹, Matthias Peter¹ and Benoît Kornmann^{1,2}✉

The distinct activities of organelles depend on the proper function of their membranes. Coordinated membrane biogenesis of different organelles necessitates lipid transport from their site of synthesis to their destination. Several factors have been proposed to participate in lipid distribution, but despite its basic importance, in vivo evidence linking the absence of putative transport pathways to specific transport defects remains scarce. A reason for this scarcity is the near absence of in vivo lipid trafficking assays. Here we introduce a versatile method named METALIC (Mass tagging-Enabled TrAcking of Lipids In Cells) to track interorganelle lipid flux inside cells. In this strategy, two enzymes, one directed to a ‘donor’ and the other to an ‘acceptor’ organelle, add two distinct mass tags to lipids. Mass-spectrometry-based detection of lipids bearing the two mass tags is then used to quantify exchange between the two organelles. By applying this approach, we show that the ERMES and Vps13-Mcp1 complexes have transport activity in vivo, and unravel their relative contributions to endoplasmic reticulum-mitochondria lipid exchange.

Organelle function depends on lipids that constitute their membranes. Membrane lipids not only constitute structural barriers but recruit specific proteins and store energy. As lipid biosynthesis in eukaryotic cells mostly happens in the endoplasmic reticulum (ER), lipids must be transported to all other cellular membranes. Lipid transport was thought to be a by-product of vesicular trafficking, but the past decade has revealed that cells have evolved non-vesicular mechanisms to mediate the bulk of lipid exchange¹. Although this transport mode is associated with all organelles, it is especially relevant for organelles like mitochondria that are excluded from vesicular traffic.

Non-vesicular lipid exchange occurs at sites of close contact (10–30 nm) between organelles, where lipid transport proteins (LTPs) solubilize lipids from membranes, shield them from the aqueous milieu in a hydrophobic pocket and catalyse their exchange between the two membranes. In yeast, the ER-mitochondria encounter structure (ERMES) is a complex of such LTPs implicated in ER-mitochondria lipid exchange^{2–8}. Three subunits, namely Mmm1, Mdm12 and Mdm34, harbour a lipid-solubilizing synaptotagmin-like mitochondrial lipid-binding protein (SMP) domain. Surprisingly, ERMES deficiency, though resulting in phenotypes including slow growth and defective mitochondrial morphology, does not prevent ER-mitochondria lipid exchange^{2,9}. Another LTP implicated in mitochondrial lipid transport is the conserved chorein-*N* motif-containing protein Vps13, which associates with mitochondria via Mcp1 refs. ^{10–12}. ERMES inactivation when combined with *vps13* or *mcp1* deletion leads to synthetic lethality^{11,13}, suggesting that Vps13 partially compensates absence of ERMES. However, although ERMES and Vps13 exhibit lipid transport activity in vitro^{3–5,14}, their redundant role in lipid exchange remains to be proven in vivo.

Despite multiple LTPs identified at membrane contact sites, our knowledge on lipid transport and LTP function in vivo remains poor, mainly due to limitations in existing tools. Our understanding of phospholipid transport is mainly derived from two methods: (1) in vivo assays using radiolabelled precursors, and (2) in vitro lipid exchange assays^{14–17}. In typical in vivo assays, cells

treated with ³H-serine produce ³H-phosphatidylserine (PS) via the PS-synthesizing enzyme in the ER. As the PS decarboxylase Psd1 produces phosphatidylethanolamine (PE) from PS in the inner mitochondrial membrane (IMM) and the methyltransferases Cho2 and Opi3 make phosphatidylcholine (PC) from PE exclusively in ER, detection of ³H-PE and ³H-PC reflects ER-mitochondria lipid exchange. This assay has limitations. First, it is limited to ER and mitochondria. Second, phospholipases might release labelled lipid headgroups, which can be re-incorporated into phospholipids via the Kennedy pathway, independent of interorganelle lipid transport. Finally, a fraction of Psd1 is localized to the ER in addition to the IMM¹⁸, weakening this assay's validity. Although in vitro assays monitoring lipid exchange between liposomes^{14,17} are useful to test the activity of LTPs implicated in lipid transport, they do not inform about lipid exchange rates, identity, origin and destinations, and regulation of transport routes in vivo.

In this Technical Report, to address these limitations, we have developed an assay called METALIC (Mass tagging-Enabled TrAcking of Lipids In Cells) that exploits enzyme-mediated mass tagging to measure the exchange of specific lipids between two organelles in vivo. Using this approach, we unravel lipid transport activity of Vps13 and ERMES in vivo and quantify their relative contributions in ER-mitochondria lipid exchange.

Results

Principle of the METALIC assay. In METALIC, a lipid-modifying enzyme is targeted to a ‘donor’ compartment of interest where it chemically modifies lipids, introducing a diagnostic ‘mass tag’. Upon transport to an ‘acceptor’ compartment, mass-tagged lipids encounter a second enzyme that introduces a different mass tag. The detection of doubly mass-tagged lipids by mass spectrometry (MS) thus serves as a proxy to monitor lipid transport between the two compartments.

Importantly, this approach can be combined with metabolic labelling to capture the kinetics of lipid transport. Pulse labelling with deuterated precursors can be used to assess the appearance kinetics of not only the doubly mass-tagged lipids but also the singly

¹Institute of Biochemistry, Department of Biology, ETH Zurich, Zurich, Switzerland. ²Department of Biochemistry, University of Oxford, Oxford, UK.

³Present address: Department of Biology, University of Fribourg, Fribourg, Switzerland. ✉e-mail: arun.johnpeter@unifr.ch; benoit.kornmann@bioch.ox.ac.uk

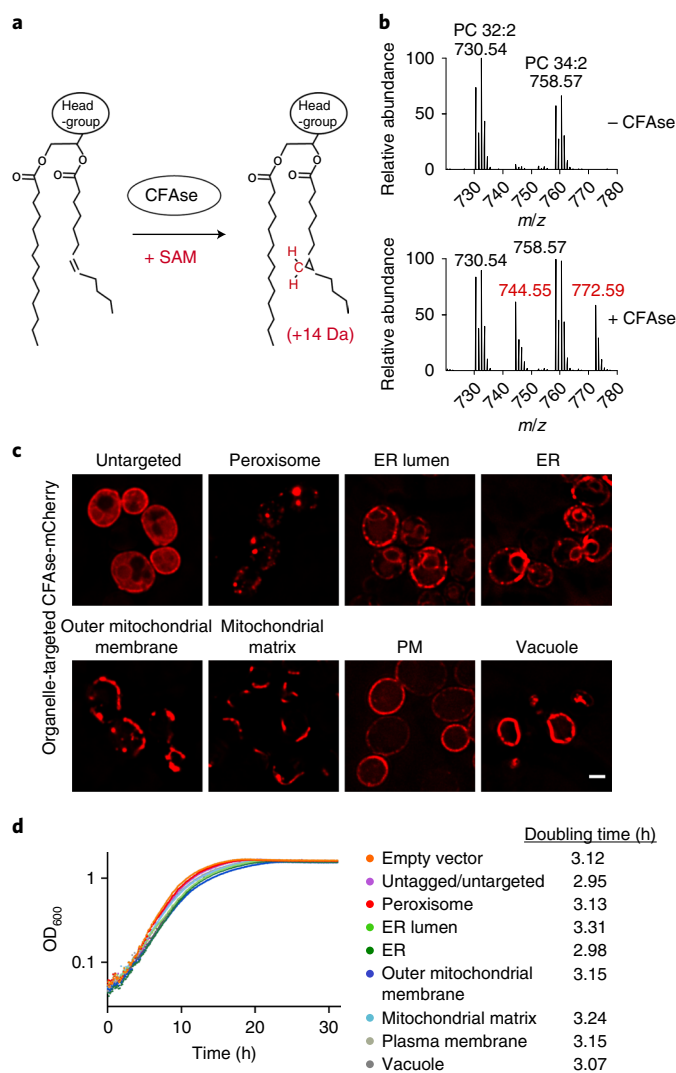


Fig. 1 | CFase is active and targetable in yeast. **a**, Scheme depicting the CFase reaction. CFase adds a methylene group (depicted in red) to double bonds on fatty acyl chains in phospholipids irrespective of their headgroup, using SAM as a co-factor, resulting in a +14 Da mass shift. **b**, CFase is active in yeast. Mass spectrum showing PC species PC 32:2 (730.54 m/z) and PC 34:2 (758.57 m/z) and their mass tagging (m/z values in red) upon expression of CFase in yeast. **c**, Localization of mCherry-tagged CFase to different organelles by fusion to targeting sequences (Methods). Scale bar, 2 μm . Similar results were obtained in three independent experiments. **d**, Semi-log plot of the growth of yeast cells expressing mCherry-tagged CFase constructs targeted to different organelles. Growth was monitored by OD_{600} measurements. Doubling time for each construct is indicated in hours. For each construct, growth was monitored for three independent clones. Source numerical data are available in source data.

labelled mass tags separately, a proxy for the activity of each enzyme and the metabolic activity of the cell.

CFase is active and targetable in yeast. We used cyclopropane-fatty-acyl phospholipid synthase (CFase), a soluble bacterial enzyme that introduces a methylene group ($-\text{CH}_2-$) from *S*-adenosyl methionine (SAM) at double bonds in phospholipid fatty acyl chains, forming a cyclopropane ring (Fig. 1a)¹⁹. Cyclopropane lipids have similar biophysical properties as their unsaturated counterparts²⁰, but carry an identifiable +14 Da mass tag (Fig. 1a). We expressed CFase constitutively in yeast and measured cyclopropylation of the

most abundant phospholipid species, PC, by MS. The mass spectrum revealed the appearance of peaks 14 Da heavier than the precursor PC species, confirming the enzyme's activity in yeast (Fig. 1b). The modified lipids represented up to 50% of any species. To test if CFase can be targeted to specific organelles, we fused targeting sequences (Methods) to a CFase-mCherry construct, verified proper localization by microscopy (Fig. 1c) and expression by western blotting (Fig. 2a). Expression of CFase in organelles did not affect growth, demonstrating that cells tolerated cyclopropane fatty acids (CFA) at the tested organelles (Fig. 1d).

To check if CFA were degradable in yeast, we fed cells with CFA (C17:0) and deuterated oleic acid (d-C18:1) (Extended Data Fig. 1a). Both fatty acids incorporated in phospholipids (Extended Data Fig. 1c). Then we removed the fatty acids from the medium and starved cells from glucose to induce fatty acid breakdown (Extended Data Fig. 1a). Free C17:0 and d-C18:1 fatty acids had a similar decay profile, comparable to the endogenous oleic acid C18:1 (Extended Data Fig. 1b). This decay was neither due to sequestration of fatty acids in phospholipids, as CFA-PE did not enrich over time (Extended Data Fig. 1c), nor to dilution by newly synthesized lipids, as the biomass remained constant during glucose starvation (Extended Data Fig. 1d). Taken together, these results suggest the half-life of CFA is similar to their unsaturated precursors.

CFase mass-tags various phospholipids in organelles. To assay organelle-targeted CFase activity, we quantified whole-cell PS, PE, PC, phosphatidylinositol (PI) and phosphatidylglycerol (PG) in wild-type cells using MS. In all cases, we could detect cyclopropylated (+14 Da) lipids (Fig. 2b). Both organelle-specific and distinct patterns were detected. Strikingly, in cells expressing mitochondria matrix-targeted CFase, CFA-PG and CFA-PE represented the highest fraction relative to other phospholipid species, in line with their precursors being synthesized in the IMM. CFA modification was variable depending on targeting, but did not correlate with CFase expression (Fig. 2a). In particular, CFase targeted to the ER lumen was less efficient than that to the cytosolic side of the ER despite being more expressed. This lower activity in the lumen could reflect differences in SAM concentration. Indeed, SAM levels in the endomembrane are unknown. We excluded the possibility that labelling by ER lumen-targeted CFase was due to a minor fraction of untranslocated enzyme as the labelling profile was distinct from untargeted CFase (Extended Data Fig. 2). In most cases, modified lipids originating from precursors with two double bonds were more abundant than those with a single double bond, consistent with two unsaturated fatty acids having double the chance for CFase modification. Interestingly, the relative abundance of CFA-PE 32:2, 32:1 and 34:2 was comparable in all compartments except mitochondrial matrix, where tagging of mono-unsaturated 32:1 species dominated over the 32:2 and 34:2 species. On the other hand, the relative abundance profile for PC followed the order 32:2 > 34:2 > 32:1 > 34:1 irrespective of the organelle, thus mimicking the abundance observed in the whole cell lipidome of yeast cells²¹. Therefore, substrate abundance can explain differences in modification efficiency. Taken together, these results demonstrate that the bacterial CFase can specifically and efficiently tag phospholipids in organelles.

Strategy to monitor ER-mitochondria lipid exchange in vivo. To monitor ER-mitochondria lipid transport, we utilized the exclusive ER localization of the PE methyltransferases Cho2 and Opi3 to introduce one of the two mass tags. We targeted CFase to the mitochondrial matrix to introduce the other mass tag. As both CFase and the methyltransferases use SAM as a methylene or methyl donor, respectively, we pulse-labelled cells with deuterated methionine (d-methionine)²¹ and monitored the appearance of both singly and doubly labelled phospholipids, the latter being indicative of lipid transport between the ER and mitochondria (Fig. 3a-c).

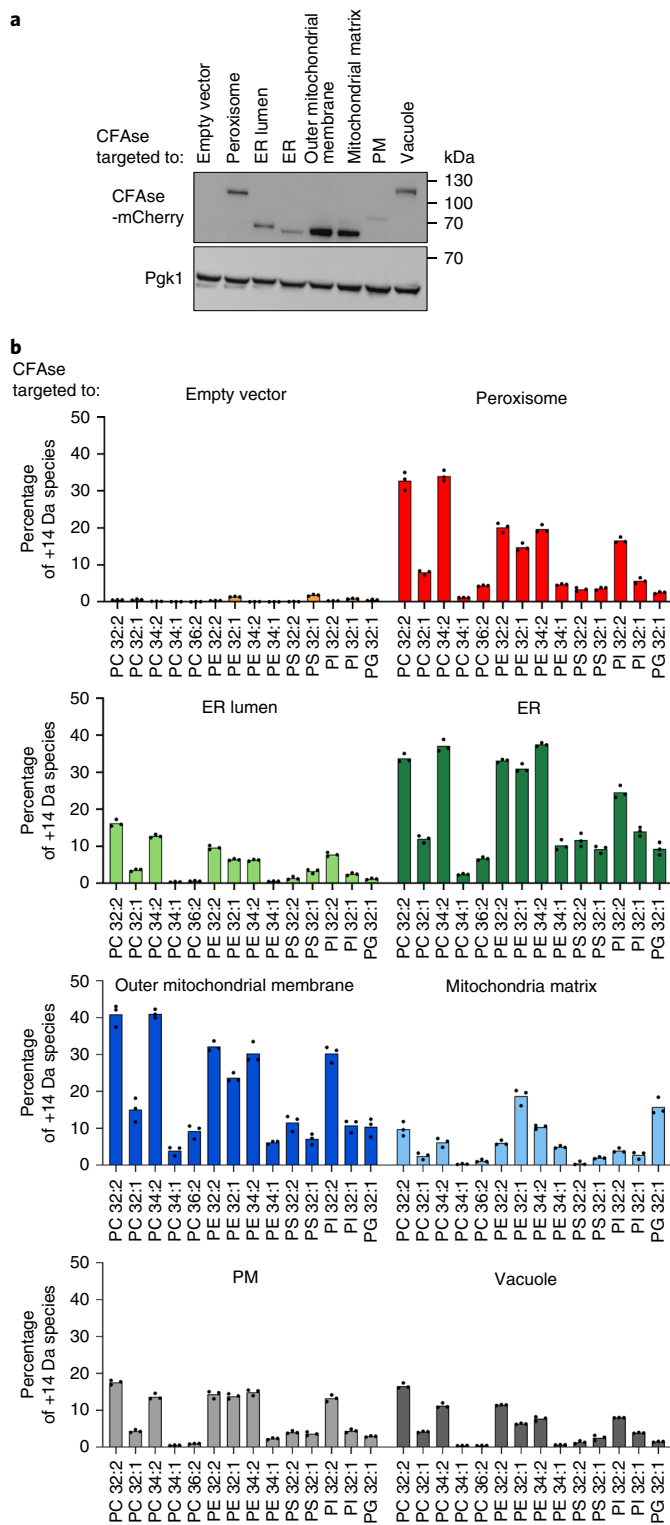


Fig. 2 | CFase mass-tags various phospholipid species in organelles. **a**, Western blot depicting levels of mCherry-tagged CFase when targeted to different organelles; similar results were obtained in three independent experiments. **b**, Bar plot showing the percentage of each indicated phospholipid species that is mass-tagged upon constitutive expression of organelle-targeted CFase in yeast. Empty vector refers to a plasmid lacking the CFase coding sequence. Percentage values represent the mean derived from experiments done on three independent clones. Source numerical data and unprocessed blots are available in source data.

As for the singly labelled species, we monitored the +9Da PC species resulting from the triple methylation of the headgroup at the ER (three deuterated -CH₃ groups being 9Da heavier than three non-deuterated ones), and the +16Da PC species resulting from cyclopropylation of PC at mitochondria. The doubly labelled species has a +25Da (9 + 16) mass shift (Fig. 3b), which can either result from the headgroup-labelled PC transported to mitochondria (Fig. 3a, route 1) or cyclopropane-labelled PE transported to the ER (Fig. 3a, route 2). Our measurements thus assess both transport directions.

Upon pulse labelling in wild-type cells, we observed a time-dependent increase in the fraction of deuterated headgroups and deuterated cyclopropanes, among the most abundant PC species (that is, 32:2, 32:1 and 34:2; Fig. 3c, red line). While incorporation of deuterated headgroups saturated close to 100%, deuterated cyclopropanes in PCs saturated at lower values, consistent with the fact that CFase modifies only a fraction of lipids (Fig. 2). The appearance kinetics of deuterated headgroups and deuterated CFAs was consistent with a model where lipid synthesis accommodates the requirement for biomass increase (as assessed by the change in optical density at 600 nm (OD₆₀₀), Extended Data Fig. 3a–d). The *t*_{3.5} timepoint was usually the most discrepant, probably stemming from the fact that the d-methionine labelling at *t*₀ involves a sudden tenfold increase in methionine availability to which cells might need to adapt.

For all major PC species, the fraction of +25Da double-labelled lipids increased over time (Fig. 3c, red line), indicative of ER–mitochondria lipid transport, the kinetics of which was again consistent with expectations (that is, corresponding to the product of deuterated headgroup and cyclopropane fractions; Extended Data Fig. 3e).

To validate the specificity of this strategy, we tested its dependency on Sam5, the major transporter of SAM across the IMM²². As CFase activity is dependent on SAM in the mitochondrial matrix, our prediction was that, in the *sam5* mutant, mass labelling should be severely impaired. Indeed, while headgroup labelling at ER was similar to wild type (the small difference might be accounted for by a slower growth rate of *sam5*Δ mutants), the incorporation of deuterated cyclopropane as well as double mass labelling was severely reduced in *sam5*Δ mutant cells (Fig. 3c, grey line). While some incorporation was observed in early timepoints, consistent with the notion that early incorporation data are perturbed by cellular adaptation to high methionine, cyclopropane incorporation returned to background levels at later timepoints, confirming near-complete CFase targeting to the mitochondrial matrix with little activity outside it. Taken together, these results highlight the robustness and sensitivity of METALIC for monitoring ER–mitochondria phospholipid exchange in vivo.

An AID system to inactivate ERMES. To assess the redundant roles of ERMES and Vps13–Mcp1 complexes in lipid exchange, we sought to assay lipid transport upon inactivation of both pathways. As co-deletion is synthetically lethal, we built an inducible system to acutely inactivate ERMES. We C-terminally fused Mdm12 to an auxin-inducible degron (AID)²³ and expressed AtTIR1, a plant auxin-dependent adapter for E3 ubiquitin ligases. One hour of auxin treatment efficiently depleted Mdm12-AID (Fig. 4a), causing typical morphological changes in mitochondria (Fig. 4b), which was unhindered by the loss of Vps13 or Mcp1 (Fig. 4d). Finally, in the presence of auxin, cells expressing Mdm12-AID grew slower, and this was exacerbated by concomitant deletion of *VPS13* or *MCP1* (Fig. 4c) as expected^{11,13,24}. These results confirm that auxin-dependent Mdm12 depletion rapidly inactivates ERMES, allowing to test its lipid transport activity in vivo using the METALIC assay.

Both ERMES and Vps13 contribute to phospholipid exchange. To unravel the roles of ERMES and Vps13–Mcp1 complexes in ER–mitochondria lipid exchange, we pulse-labelled cells with

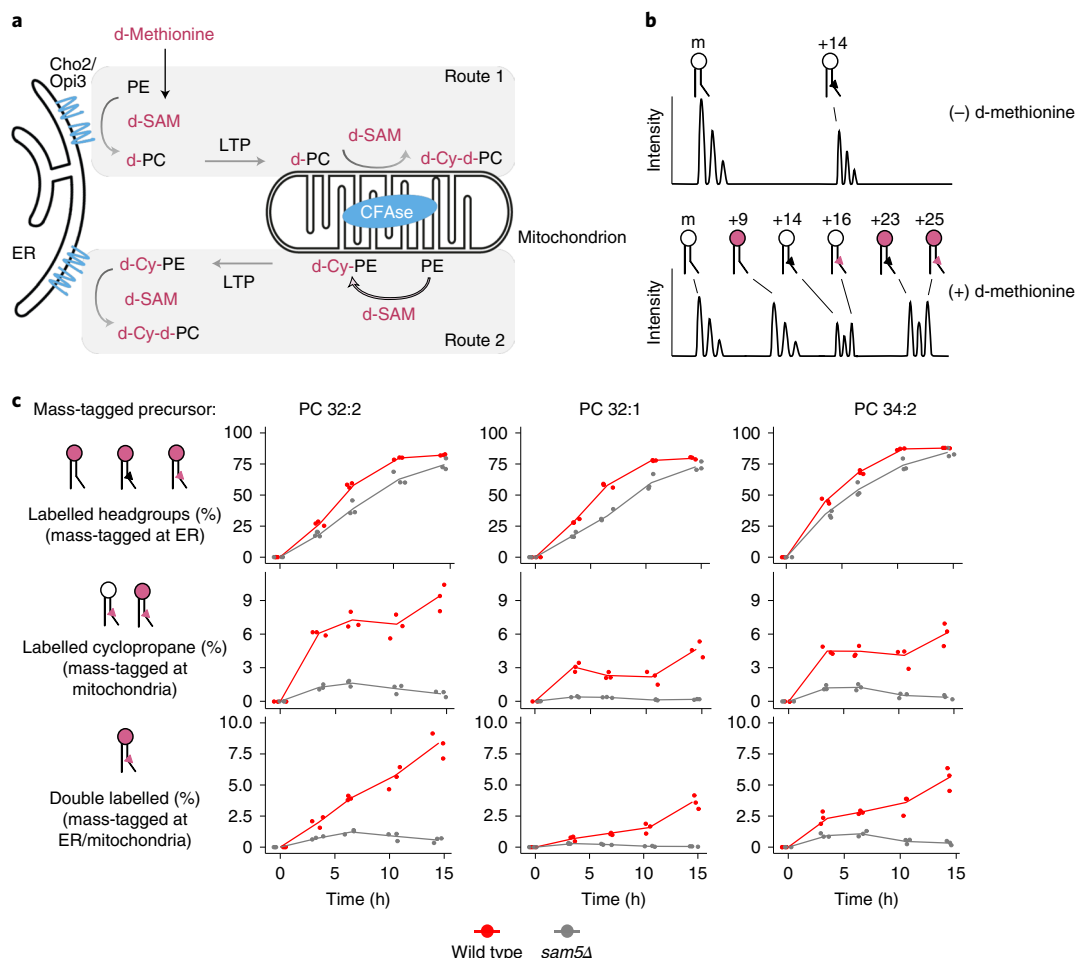


Fig. 3 | Monitoring ER-mitochondria lipid exchange using METALIC. **a**, CFase is targeted to the mitochondrial matrix, while the endogenous methyltransferases Cho2 and Opi3 localize to the ER. These enzymes at the two organelles serve to introduce distinct mass tags. Cells are pulse-labelled with *d*-methionine, resulting in deuterated SAM (*d*-SAM). In Route 1, the first mass tagging occurs in ER, resulting in *d*-PC (+9 Da). When *d*-PC is transported by an LTP to the mitochondrial matrix, a second mass tag (+16 Da) in the form of a deuterated cyclopropane group (*d*-Cy) is added by CFase using *d*-SAM, resulting in *d*-Cy-*d*-PC (+25 Da). The doubly mass-tagged species can also result from Route 2, where PE in the mitochondrial matrix can get a deuterated cyclopropane mass tag (+16 Da), which subsequently can be double mass-tagged (+9 Da) in the ER by the methyltransferases. **b**, Theoretical mass spectra illustrating the different modifications of a precursor PC species. At steady state, in addition to the precursor, only the cyclopropylated +14 Da species (black triangle) is detected owing to the constitutive expression of CFase. Upon treatment with *d*-methionine, labelling of the headgroup at the ER (pink headgroups) results in the +9 Da shift. Headgroup labelling of the +14 Da species results in the detection of +23 Da species. Detection of +16 Da species indicates the labelling of the tail in PCs at mitochondria (red triangle). Double mass labelling of both the headgroup (at ER) and the tail (at mitochondria) result in a +25 Da mass tag. **c**, Line plot depicting the percentage of incorporation in the headgroup (sum of +9, +23 and +25 species), fatty acid tail (sum of +16 and +25 species) and both (+25 species) after *d*-methionine pulse labelling of cells of the indicated genotype at the indicated timepoints. Three independent clones for each genotype were used. Source numerical data are available in source data.

d-methionine and assayed mass-tag labelling upon inactivation of either one or both pathways (Fig. 5a). Headgroup-labelling kinetics was similar in all the LTP mutants, indicating that, despite different growth phenotypes, cells are metabolically active and generate new PC headgroups at comparable rates (Fig. 5b,c, top).

To address the contribution of the Mcp1-Vps13 pathway alone to lipid transport, we assayed mass-tag labelling in *MDM12-AID mcp1Δ* cells, without auxin (–auxin) to maintain ERMES function (Fig. 5b). First, we quantified all species with deuterated headgroup or cyclopropane rings with the exception of doubly mass-labelled species, to assess label incorporation independent of transport. While we observed a similar increase in headgroup labelling, increased modification of the cyclopropane ring was transient, probably reflecting faster labelling at the headgroup than at the cyclopropane ring, and thus by the end of the experiment most PC

molecules bore deuterated headgroups. As shown in Fig. 5b, *MCP1* deletion alone impacted neither headgroup nor cyclopropane labelling. We then quantified doubly mass-labelled lipids (+25 Da), indicative of ER–mitochondria lipid exchange. In this set-up, doubly mass-labelled species increased monotonously in *MDM12-AID* (surrogate wild type) and *MDM12-AID mcp1Δ* cells. While PC 32:2 was not affected, after 14.5 h, there was a mild (25%) but significant reduction in double mass labelling of PC 32:1 ($P = 0.038$) and a non-statistically significant reduction in PC 34:2 ($P = 0.32$) (Fig. 5b, bottom).

To assess the role of ERMES, we treated cells bearing *MDM12-AID* with auxin for 7 h before pulse labelling (Fig. 5a and Extended Data Fig. 4). While headgroup and cyclopropane labelling was unaffected, double mass labelling (+25 Da species) was reduced (Fig. 5c, red lines), especially for the PC 32:2 species.

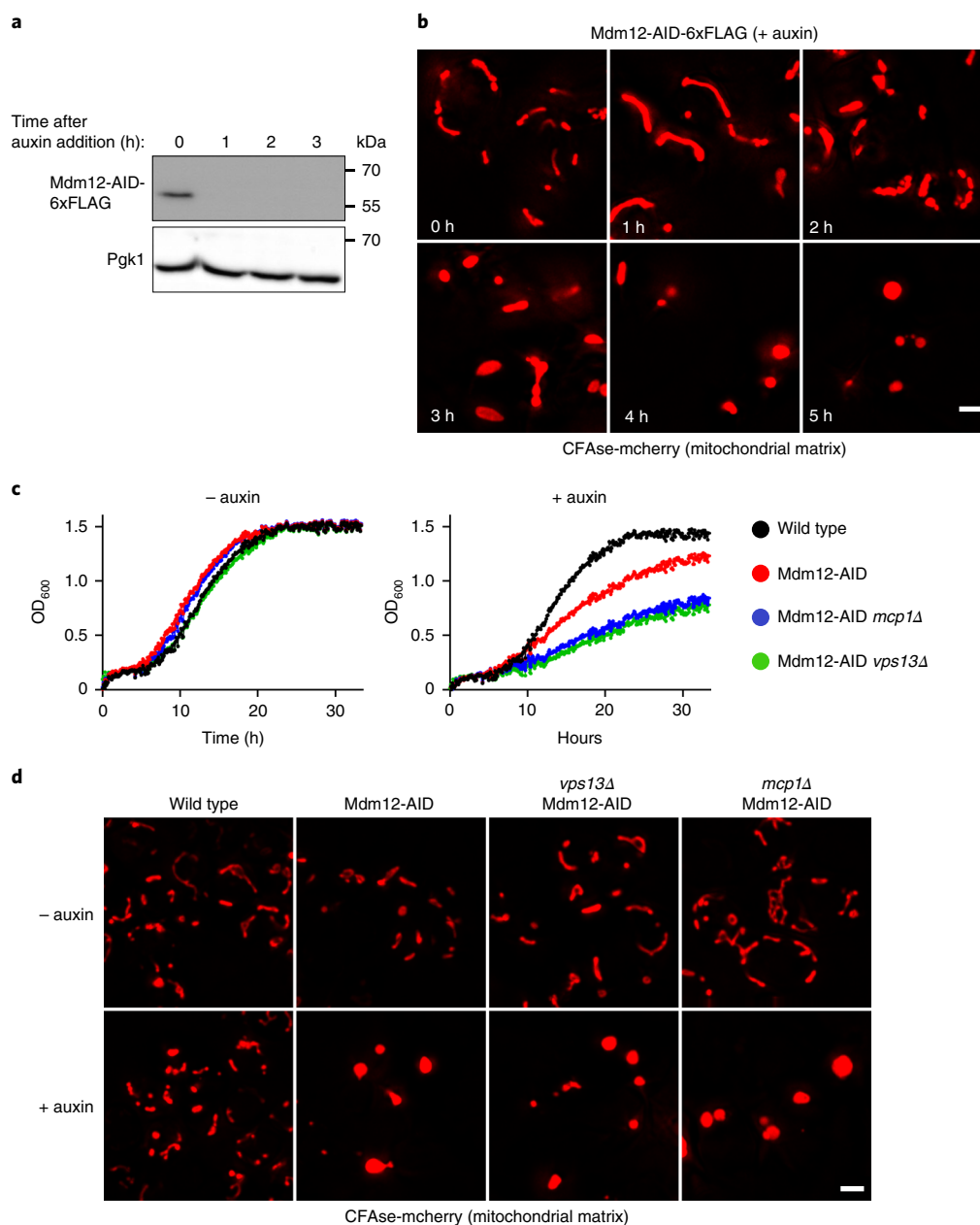


Fig. 4 | An AID system to inactivate ERMES. **a**, Cells co-expressing AtTIR-9xMyc and Mdm12-AID-6xFLAG were treated with 0.5 mM auxin, grown at 30 °C and collected at defined timepoints (h). Total protein extracts were analysed by SDS-PAGE and western blotting. Mdm12 was detected using an α -FLAG antibody. Phosphoglycerate kinase, which serves as a loading control, was detected using an α -PGK antibody; similar results were obtained in two independent experiments. **b**, Cells bearing the Mdm12 degron system and expressing the mitochondria matrix-targeted CFase were treated with 0.5 mM auxin and imaged at the mentioned timepoints (h). Images correspond to a maximum-intensity projection of six Z-slices. Similar results were obtained in three independent experiments. Scale bar, 2 μ m. **c**, Growth of cells with the indicated genotypes was monitored using OD₆₀₀ measurements in the absence or presence of 0.5 mM auxin. **d**, Localization of mCherry-tagged CFase in the indicated strains, either in the absence of auxin or upon treatment with 0.5 mM auxin for 7 h. Similar results were obtained in three independent experiments. Scale bar, 2 μ m. Source numerical data and unprocessed blots are available in source data.

Finally, we assessed mass tagging in *MDM12-AID* cells with either *VPS13* or *MCP1* deleted. We observed a slight reduction in headgroup and cyclopropane labelling (at least for the PC32:1 species; Fig. 5c, blue and green lines). Strikingly, however, double mass labelling was reduced close to background levels by co-inactivation of ERMES and either *Vps13* or *Mcp1*, particularly for PC 32:1.

Thus, while both pathways might show some specificity with regard to the transported phospholipids, these results demonstrate

that ERMES and *Vps13-Mcp1* complexes function in ER-mitochondria lipid exchange *in vivo*, providing a biochemical basis for their genetic redundancy.

CFase mass-tags phospholipids in mammalian cells. To assess if METALIC could be used in higher eukaryotes, we expressed various mCherry-tagged organelle-targeted CFase constructs in HeLa cells under the control of a doxycycline-inducible promoter by lentiviral transduction. Immunofluorescence and western blotting

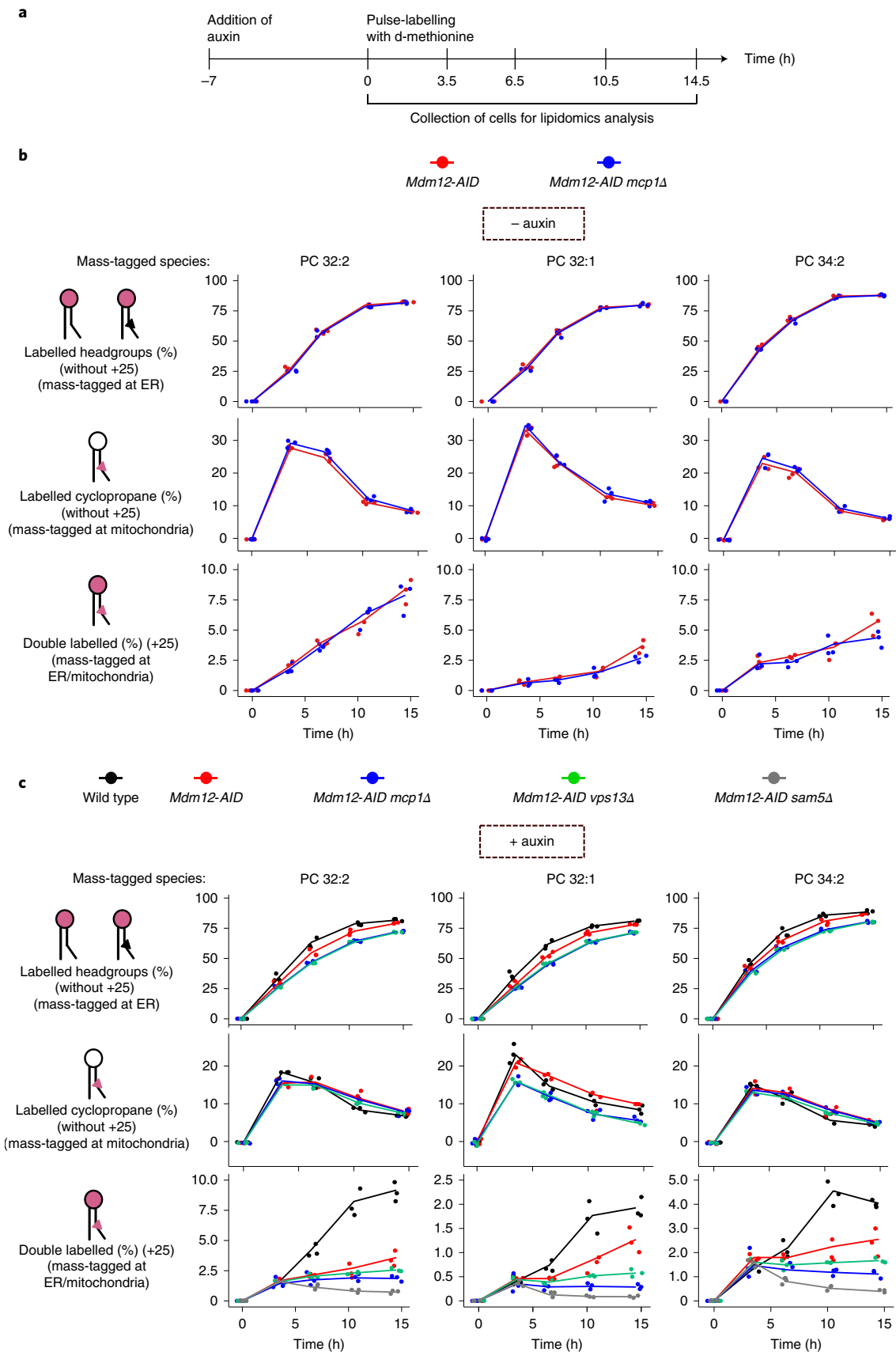


Fig. 5 | Kinetics of ER-mitochondria phospholipid exchange. **a**, Depiction of the timepoints at which cells were collected for lipidomics analysis upon pulse labelling with d-methionine, after treatment with 0.5 mM auxin for 7 h. **b, c**, Line plots showing the fraction of the +9 Da, +16 Da and +25 Da species over time in the indicated genotypes either without (**b**) or with (**c**) auxin treatment. Three independent clones of each genotype were used. Source numerical data are available in source data.

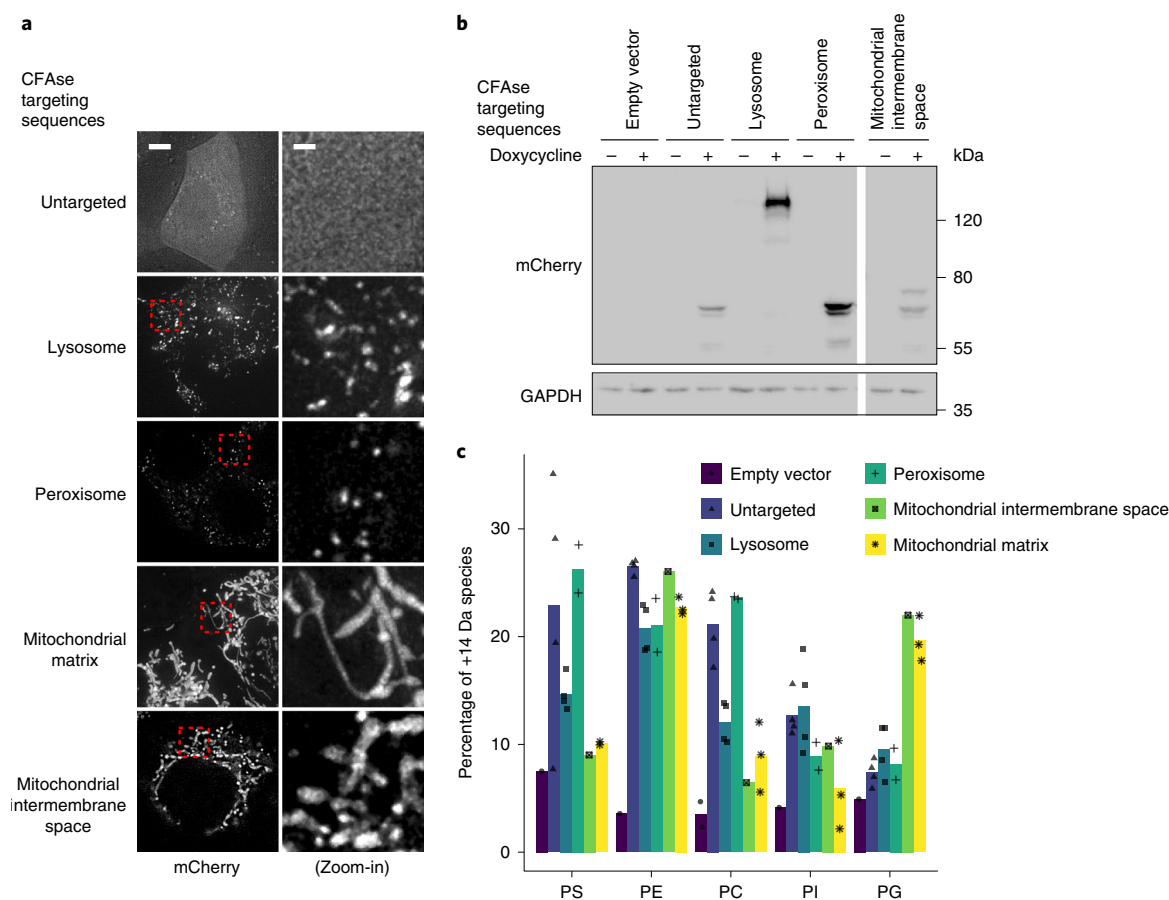


Fig. 6 | CFase mass-tags phospholipids in mammalian cells. **a**, Localization of mCherry-tagged CFase to different organelles by fusion to targeting sequences (Methods). Scale bars, 5 μ m (left) and 1 μ m (right). Similar results were obtained in at least two independent experiments. **b**, Western blot depicting levels of mCherry-tagged CFase when targeted to different organelles. This experiment was performed once, but similar results were obtained and are shown in Extended Data Fig. 5a. **c**, Bar plot showing the percentage of mass-tagged lipid averaging for each detectable species of the indicated phospholipid class upon constitutive expression of organelle-targeted CFase in HeLa cells. Empty vector refers to a plasmid lacking the CFase coding sequence. Source numerical data and unprocessed blots are available in source data.

confirmed proper localization and expression (Fig. 6a,b and Extended Data Fig. 5a). Liquid chromatography (LC)–MS showed that lipids with mass consistent with cyclopropylation could be detected even in cells expressing no CFase. This is probably due to the presence of ether-linked plasmalogen lipids, containing fatty alcohols that are 14 Da lighter than their fatty acid counterpart with same carbon number. Thus, a C16 fatty acid with cyclopropane modification (C17) has a molecular weight identical to a C18 fatty alcohol. Nevertheless, we observed an increase in abundance of species corresponding to cyclopropane lipids for most constructs and most lipids (Fig. 6c). The changes observed were consistent with the enzyme’s subcellular localization. For instance, CFase targeted to either the mitochondrial matrix or intermembrane space was most efficient at modifying PG, a lipid virtually exclusively found in mitochondrial membranes. By contrast, the same constructs were very inefficient at modifying PS, a lipid that is rare in mitochondrial membranes. Importantly, expression of the enzyme and lipid modification did not affect cell survival as assessed by Trypan Blue staining (Extended Data Fig. 5b). Together these data indicate that CFA synthase can be utilized to modify lipids in an organelle-specific way in higher eukaryotes.

Discussion

Here we demonstrate the utility of METALIC, a versatile strategy to probe interorganelle lipid transport in vivo using ER–mitochondria

as a model organelle pair. Our survey ties up hampering loose ends in our understanding of ER–mitochondria lipid exchange. It demonstrates the contribution of two candidate pathways, for which direct in vivo evidence had thus far been missing or incomplete^{2–5,8,25}. We observe that the Vps13–Mcp1 pathway contributes minimally to ER–mitochondria lipid exchange, correlating with the observation that neither *VPS13* nor *MCP1* deletion affects mitochondria morphology or yeast growth. On the other hand, contribution of ERMES to lipid transport is substantial, in line with the strong mitochondrial and growth phenotypes of *ermes* mutants. Moreover, the two pathways function in a redundant fashion, accounting for the bulk of lipid transport between the two organelles, potentially explaining the synthetic lethality of mutants lacking them.

Interestingly, the lipid transport defect in *ermes* mutants is particularly striking for doubly unsaturated species 32:2 and 34:2. By contrast, the 32:1 species was most affected in *ermes vps13* or *ermes mcp1* double-mutant cells. In fact, transport of this lipid was modestly but significantly affected by the loss of *MCP1* alone. Together, these findings suggest that lipid-binding pockets of LTPs could have preferences for specific fatty acids.

The fact that CFase can be directed to multiple compartments makes it possible to study phospholipid transport between ER and any organelle of interest, as long as targeting is stringent. In the case of mitochondrial matrix, both microscopy and the analysis of the *sam5Δ* mutant indicates that mistargeting of CFase is negligible.

In fact, we do not know if the residual activity of matrix-directed CFAse in the *sam5Δ* mutant is due to partial enzyme mistargeting or residual mitochondrial membrane permeability to SAM in the absence of Sam5.

Our data show that cyclopropane lipids can be synthesized and transported in yeast and human cells without perturbing their function. The approach is complicated in mammalian cells by plasmalogens with the same *m/z* as cyclopropane-modified lipids. This limitation could be overcome by using tandem MS, which could detect different fragmentation product for plasmalogen and cyclopropane lipids, or other LC approaches to discriminate the two types. Of note, *Caenorhabditis elegans* worms feeding on bacteria incorporate CFA into their lipidome^{26,27}, indicating that CFAse can probably be used in invertebrate systems. Therefore, even if their behaviour is not identical to unsaturated lipids, cyclopropane lipids can serve as useful tools within the METALIC approach to assay lipid transport, and unravel relative differences in different genetic backgrounds (lipid-transport mutants) or physiological conditions. In addition to MS-based methods, CFA lipids can be detected by Raman spectroscopy, potentially allowing single-cell resolution²⁸.

One limitation of the enzymes chosen here is their requirement for SAM. Most of the known SAM-requiring enzymes in yeast have active sites in the cytoplasm, nucleus or mitochondria²⁹, suggesting that SAM might not be available in the lumen of other organelles. Our results indicate that ER-lumen-targeted CFAse can modify lipids in this compartment (Fig. 2). In addition, SAM levels in the lumen of endocytic compartments can probably be manipulated by adding SAM to the culture medium, which can be endocytosed by bulk flow. Nevertheless, to overcome the issue of SAM availability, we chose to target most CFAse constructs to organelles' cytosolic face (Fig. 1c). Whether enzymes tethered to a membrane's cytosolic side might act on other membranes *in trans* at interorganelle contacts needs to be verified for chosen organelle pairs. Another limitation of the approach is that it does not inform on transport directionality (Fig. 3a, Route 1 versus Route 2), nor whether it is direct or involves intermediate compartments, as is probably the case for the Mcp1–Vps13 pathway. Therefore, any rate calculated with METALIC cannot be used as a direct measure of lipid exchange. However, the effect of perturbations on lipid traffic can be measured with METALIC, as we show here for ER–mitochondria lipid transport. One obvious caveat of enzyme-based methods is that any perturbation can affect either lipid transport or mass-tag incorporation. In METALIC, the incorporation rates by both enzymes can be surveyed independently and used to normalize the rate of appearance of the doubly mass-tagged (and therefore transported) species.

The involvement of multiple redundant LTPs in interorganelle lipid transport appears to be the rule rather than the exception. Indeed, among ~40 putative LTPs identified in yeast, none is truly essential for growth, indicating redundant mechanisms at play. Here we study two pathways allowing exchange of lipids between mitochondria and the endomembrane system. While the ERMES complex localizes to ER–mitochondria contacts and, therefore, probably catalyses direct lipid exchange between the two compartments, Vps13–Mcp1 has been found at mitochondria–vacuoles^{11,13} and mitochondria–endosome contacts²⁴. The various localization of these complexes indicates that lipids can use alternate routes that may or may not involve intermediate organelles, to transit from their synthesis site to their destination. The direct versus indirect nature of the transport pathways, in addition to the intrinsic preferences of different LTPs, might explain potential lipid specificities observed here. Deciphering the contribution of these many LTPs, their redundancy and their preferences therefore constitutes an important challenge in cell biology. However, despite the central contribution of lipids to many cellular functions, our knowledge lags behind DNA, RNA and proteins, as we do not have the equivalent tools (PCR and green fluorescent protein tagging). The development of METALIC

thus takes an important step forward and paves the way to elucidate LTP function and lipid transport processes *in vivo*.

Online content

Any methods, additional references, Nature Research reporting summaries, source data, extended data, supplementary information, acknowledgements, peer review information; details of author contributions and competing interests; and statements of data and code availability are available at <https://doi.org/10.1038/s41556-022-00917-9>.

Received: 1 September 2021; Accepted: 18 April 2022;

Published online: 2 June 2022

References

- Wong, L. H., Gatta, A. T. & Levine, T. P. Lipid transfer proteins: the lipid commute via shuttles, bridges and tubes. *Nat. Rev. Mol. Cell Bio* **20**, 85–101 (2019).
- Kornmann, B. et al. An ER–mitochondria tethering complex revealed by a synthetic biology screen. *Science* **325**, 477–481 (2009).
- Kawano, S. et al. Structure–function insights into direct lipid transfer between membranes by Mmm1–Mdm12 of ERMES. *J. Cell Biol.* **217**, 959–974 (2018).
- Kojima, R., Endo, T. & Tamura, Y. A phospholipid transfer function of ER–mitochondria encounter structure revealed *in vitro*. *Sci. Rep.* **6**, 30777 (2016).
- AhYoung, A. P. et al. Conserved SMP domains of the ERMES complex bind phospholipids and mediate tether assembly. *Proc. Natl Acad. Sci. USA* **112**, E3179–E3188 (2015).
- AhYoung, A. P., Lu, B., Cascio, D. & Egea, P. F. Crystal structure of Mdm12 and combinatorial reconstitution of Mdm12/Mmm1 ERMES complexes for structural studies. *Biochem. Biophys. Res. Commun.* **488**, 129–135 (2017).
- Jeong, H., Park, J. & Lee, C. Crystal structure of Mdm12 reveals the architecture and dynamic organization of the ERMES complex. *EMBO Rep.* **17**, 1857–1871 (2016).
- Jeong, H., Park, J., Jun, Y. & Lee, C. Crystal structures of Mmm1 and Mdm12–Mmm1 reveal mechanistic insight into phospholipid trafficking at ER–mitochondria contact sites. *Proc. Natl Acad. Sci. USA* **114**, E9502–E9511 (2017).
- Burgess, S. M., Delannoy, M. & Jensen, R. E. MMM1 encodes a mitochondrial outer membrane protein essential for establishing and maintaining the structure of yeast mitochondria. *J. Cell Biol.* **126**, 1375–1391 (1994).
- Bean, B. D. M. et al. Competitive organelle-specific adaptors recruit Vps13 to membrane contact sites. *J. Cell Biol.* **217**, 3593–3607 (2018).
- John Peter, A. T. et al. Vps13–Mcp1 interact at vacuole–mitochondria interfaces and bypass ER–mitochondria contact sites. *J. Cell Biol.* **216**, 3219–3229 (2017).
- Tan, T., Özalci, C., Brügger, B., Rapaport, D. & Dimmer, K. S. Mcp1 and Mcp2, two novel proteins involved in mitochondrial lipid homeostasis. *J. Cell Sci.* **126**, 3563–3574 (2013).
- Lang, A. B., John Peter, A. T., Walter, P. & Kornmann, B. ER–mitochondrial junctions can be bypassed by dominant mutations in the endosomal protein Vps13. *J. Cell Biol.* **210**, 883–890 (2015).
- Kumar, N. et al. VPS13A and VPS13C are lipid transport proteins differentially localized at ER contact sites. *J. Cell Biol.* **217**, 3625–3639 (2018).
- Vance, J. E. Phospholipid synthesis in a membrane fraction associated with mitochondria. *J. Biol. Chem.* **265**, 7248–7256 (1990).
- Lahiri, S. et al. A conserved endoplasmic reticulum membrane protein complex (EMC) facilitates phospholipid transfer from the ER to mitochondria. *PLoS Biol.* **12**, e1001969 (2014).
- Valverde, D. P. et al. ATG2 transports lipids to promote autophagosome biogenesis. *J. Cell Biol.* **218**, 1787–1798 (2019).
- Friedman, J. R. et al. Lipid homeostasis is maintained by dual targeting of the mitochondrial PE biosynthesis enzyme to the ER. *Dev. Cell* **44**, 261–270.e6 (2018).
- Wang, A. Y., Grogan, D. W. & Cronan, J. E. Cyclopropane fatty acid synthase of *Escherichia coli*: deduced amino acid sequence, purification, and studies of the enzyme active site. *Biochemistry* **31**, 11020–11028 (1992).
- Zhang, Y.-M. & Rock, C. O. Membrane lipid homeostasis in bacteria. *Nat. Rev. Microbiol.* **6**, 222–233 (2008).
- Boumann, H. A. et al. The two biosynthetic routes leading to phosphatidylcholine in yeast produce different sets of molecular species. Evidence for lipid remodeling. *Biochemistry* **42**, 3054–3059 (2003).
- Marobbio, C. M. T., Agrimi, G., Lasorsa, F. M. & Palmieri, F. Identification and functional reconstitution of yeast mitochondrial carrier for S-adenosylmethionine. *EMBO J.* **22**, 5975–5982 (2003).
- Morawska, M. & Ulrich, H. D. An expanded tool kit for the auxin-inducible degron system in budding yeast. *Yeast* **30**, 341–351 (2013).
- Park, J.-S. et al. Yeast Vps13 promotes mitochondrial function and is localized at membrane contact sites. *Mol. Biol. Cell* **27**, 2435–2449 (2016).

25. Nguyen, T. T. et al. Gem1 and ERMES do not directly affect phosphatidylserine transport from ER to mitochondria or mitochondrial inheritance. *Traffic* **13**, 880–890 (2012).
26. Kaul, T. K., Rodrigues, P. R., Ogungbe, I. V., Kapahi, P. & Gill, M. S. Bacterial fatty acids enhance recovery from the dauer larva in *Caenorhabditis elegans*. *PLoS ONE* **9**, e86979 (2014).
27. Castro, C. et al. A metabolomic strategy defines the regulation of lipid content and global metabolism by $\Delta 9$ desaturases in *Caenorhabditis elegans*. *BMC Genomics* **13**, 36 (2012).
28. Kochan, K. et al. Raman spectroscopy as a tool for tracking cyclopropane fatty acids in genetically engineered *Saccharomyces cerevisiae*. *Analyst* **144**, 901–912 (2018).
29. Wlodarski, T. et al. Comprehensive structural and substrate specificity classification of the *Saccharomyces cerevisiae* methyltransferome. *PLoS ONE* **6**, e23168 (2011).

Publisher's note Springer Nature remains neutral with regard to jurisdictional claims in published maps and institutional affiliations.



Open Access This article is licensed under a Creative Commons Attribution 4.0 International License, which permits use, sharing, adaptation, distribution and reproduction in any medium or format, as long as you give appropriate credit to the original author(s) and the source, provide a link to the Creative Commons license, and indicate if changes were made. The images or other third party material in this article are included in the article's Creative Commons license, unless indicated otherwise in a credit line to the material. If material is not included in the article's Creative Commons license and your intended use is not permitted by statutory regulation or exceeds the permitted use, you will need to obtain permission directly from the copyright holder. To view a copy of this license, visit <http://creativecommons.org/licenses/by/4.0/>.

© The Author(s) 2022

Methods

Yeast strains and plasmids. Yeast strains, plasmids and primers used in this study are listed in Supplementary Table 1. Yeast cells were cultured at 30 °C in synthetic defined (SD) medium with 2% glucose (2% glucose, 0.5% NH₄-sulfate, 0.17% yeast nitrogen base and amino acids). Genomic integration of PCR fragments was done by homologous recombination^{30,31}. Gene deletions were confirmed by colony PCR. Growth curves were obtained using Clariostar equipped with the manufacturer's software (version 5.4). CFase open reading frame was amplified from *Escherichia coli*. A CFase-mCherry construct was targeted to different organelles using the following targeting sequences: for the ER membrane, the C-terminal 20 residues of Ubc6 (230–250); for the ER lumen, the signal sequence of Kar2 (amino acids 1–41) at the N-terminus and an HDEL signal at the C-terminus; for the outer mitochondrial membrane, amino acids 1–30 of Tom70; for the mitochondrial matrix, amino acids 1–69 of subunit 9 of the F₀-ATPase from *Neurospora crassa*; for the peroxisome, full-length Pex3 at the N-terminus; for the plasma membrane, the PH domain of Osh1 (amino acids 268–388); for the vacuole, full-length Vac8 at the N-terminus.

Mammalian cell culture. HeLa cells were cultured in MEM α medium, supplemented with 10% foetal calf serum and 1% penicillin–streptomycin. They were incubated at 37 °C and 5% CO₂. Stable cell lines were generated by lentiviral transduction as published previously³². CFase-mCherry construct was targeted to different organelles using the following targeting sequences: for lysosomal targeting, 1–407 amino acids of Lamp1 were fused N-terminally to CFase; for peroxisomal targeting, an SKL signal at the C-terminus; for mitochondrial intermembrane space targeting, the presequence of Sma1 (amino acids 1–59) at the N-terminus; for mitochondrial matrix targeting, the presequence of Cox8 (amino acids 1–35) at the N-terminus.

Microscopy. Cells were grown to mid-log phase in SD–uracil medium for selection of the mitochondrial matrix-targeted CFase-mCherry plasmid. Mammalian cells were incubated in MEM α medium containing 10% foetal calf serum and 1% penicillin–streptomycin. The expression of the CFase-mCherry constructs was induced with 1 mM doxycycline overnight. Before the imaging, the medium was exchanged with PBS.

Images were acquired using a DeltaVision MPX microscope (Applied Precision) equipped with a 100 \times 1.40 NA oil UplanS-Apo objective lens (Olympus), a multicolour illumination light source, and a CoolSNAPHQ2 camera (Roper Scientific). Image acquisition was done at room temperature. Images were deconvolved with Deltavision SoftWoRx software (version 6.5.2) using the manufacturer's parameters. Images were processed further using FIJI ImageJ (version 1.53c) bundle.

Protein extraction and western blotting. For yeast, 1 OD₆₀₀ of mid-log phase cells was collected by centrifugation and precipitated using 10% trichloroacetic acid for 20 min at 4 °C. After centrifugation at 13,000g for 5 min, pellets were washed with ice-cold acetone. Pellets were air-dried and resuspended in 30 μ l of 1 \times SDS sample buffer (60 mM Tris pH 6.8, 2% SDS, 10% glycerol, 5% 2-mercaptoethanol and 0.005% bromophenol blue), and boiled for 3 min. For mammalian cells, 10⁶ cells were scraped off in 100 μ l of SDS sample buffer and heated at 96 °C for 10 min. Samples were resolved on a 12% SDS–PAGE gel, and after transfer on a PVDF membrane, proteins were detected using specific antibodies. The following antibodies were used: mouse anti-Pgk1 antibody (Invitrogen, 459250, 1:3,000 dilution), rat anti-RFP antibody (Chromotek, 5F8, 1:1,000 dilution), mouse anti-FLAG antibody (Sigma, F1804, 1:1,000), rabbit anti-mCherry antibody (Abcam, ab167453, 1:1,000) and horseradish-peroxidase-coupled secondary antibody (Bio-Rad, 170–6516; 1:10,000 dilution). Western blots were imaged using the Fusion FX system (Vilber) equipped with the FusionCapt Advance FX7 software (version 17.03).

Pulse labelling, lipid extraction and MS analysis. Pre-cultures in SD medium were diluted to 0.8 OD₆₀₀ ml⁻¹ in 25 ml and treated with 0.5 mM auxin for 7 h. Next, cells were pulse-labelled with 2 mM d-methionine and grown at 30 °C. At the indicated timepoints, 8 OD₆₀₀ of cells was pelleted, snap-frozen and stored at –80 °C. Lipids were extracted as described previously with minor modifications³³. Briefly, cells were washed in ice-cold water and subsequently resuspended in 1.5 ml of extraction solvent containing ethanol, water, diethyl ether, pyridine and 4.2 N ammonium hydroxide (v/v 15:15:5:1:0.18). After the addition of 300 μ l glass beads, samples were vortexed vigorously for 5 min and incubated at 60 °C for 20 min. Cell debris were pelleted by centrifugation at 1,800g for 10 min, and the supernatant was dried under a stream of nitrogen. The dried extract was resuspended in 1 ml of water-saturated butanol and sonicated for 5 min in a water bath sonicator. Then, 500 μ l of water was added and vortexed further for 2 min. After centrifugation at 3,000g, the upper butanol phase was collected, dried under a stream of nitrogen and resuspended in 50% methanol for lipidomics analysis.

LC analysis was performed as described previously with several modifications³⁴. Phospholipids were separated on a nanoAcquity ultra-performance liquid chromatography unit (Waters) equipped with a HSS T3

capillary column (150 m \times 30 mm, 1.8 μ m particle size; Waters), applying a 10 min linear gradient of buffer A (5 mM ammonium acetate in acetonitrile:water 60:40) and B (5 mM ammonium acetate in isopropanol:acetonitrile 90:10) from 10% B to 100% B. Conditions were kept at 100% B for the next 7 min, followed by a 8 min re-equilibration to 10% B. The injection volume was 1 μ l. The flow rate was constant at 2.5 μ l min⁻¹.

The ultra-performance liquid chromatography unit was coupled to QExactive mass spectrometer (Thermo) by a nanoESI source (New Objective Digital PicoView 550) equipped with the Thermo QExactive XCalibur software (version 4.0.27.10). The source was operated with a spray voltage of 2.9 kV in positive mode and 2.5 kV in negative mode. Sheath gas flow rate was set to 25 and 20 for positive and negative mode, respectively. MS data were acquired using either positive or negative polarization, alternating between full MS and all-ion-fragmentation scans. Full scan MS spectra were acquired in profile mode from 107 m/z to 1,600 m/z with an automatic gain control target of 1 \times 10⁶, an Orbitrap resolution of 70,000 and a maximum injection time of 200 ms. All-ion-fragmentation spectra were acquired from 107 m/z to 1,600 m/z with an automatic gain control value of 5 \times 10⁴, a resolution of 17,500 and a maximum injection time of 50 ms, and fragmented with a normalized collision energy of 20, 30 and 40 (arbitrary units). Generated fragment ions were scanned in the linear trap. Positive ion mode was employed for monitoring PC and negative ion mode was used for monitoring PS and PE. Lipid species were identified on the basis of their m/z and elution time. We used a standard mixture comprising PS 10:0/10:0, PE 17:0/17:0, PC 17:0/17:0, PG 17:0/17:0 and PI 12:0/13:0 for deriving an estimate of specific elution times. Lipid intensities were quantified using the Skyline (version 21.2.0.369) software³⁵. For each phospholipid, signal was integrated for the precursor species (m), cyclopropane species (m₊₁₄) and species that appear upon pulse labelling with d-methionine (m₊₉, m₊₁₆, m₊₂₃ and m₊₂₅). Fraction of cyclopropylated species (Fig. 2) upon constitutive expression of CFase was calculated as (m₊₁₄)/(m + m₊₁₄). Fraction of labelled headgroups (Fig. 3), was calculated as (m₊₉ + m₊₂₃ + m₊₂₅)/(m + m₊₉ + m₊₁₄ + m₊₁₆ + m₊₂₃ + m₊₂₅). Fraction of labelled cyclopropane (Fig. 3) was calculated as (m₊₁₆ + m₊₂₅)/(m + m₊₉ + m₊₁₄ + m₊₁₆ + m₊₂₃ + m₊₂₅). Fraction of labelled headgroups and cyclopropane, independent of transport (Fig. 5), was calculated as (m₊₉ + m₊₂₃)/(m + m₊₉ + m₊₁₄ + m₊₁₆ + m₊₂₃ + m₊₂₅) and (m₊₁₆)/(m₊₁₄ + m₊₁₆ + m₊₂₃ + m₊₂₅), respectively. Fraction of doubly labelled mass-tagged species (Figs. 3 and 5) was calculated as (m₊₂₃)/(m + m₊₉ + m₊₁₄ + m₊₁₆ + m₊₂₃ + m₊₂₅). A step-by-step protocol describing the METALIC approach can be found at Protocol Exchange³⁶.

Lipid extraction and analysis for mammalian cells. A total of 10⁶ cells were scraped off, pelleted and resuspended in 125 μ l water. They were transferred to glass tubes and 250 μ l cold extraction solvent (methanol:0.1 N HCl 1:1) was added. The suspension was vortexed for 1 min before 250 μ l cold chloroform was added. After 15 min incubation, the solution was spun for 20 min at 3,500g at 4 °C. The lower phase was transferred into a fresh glass tube and dried under a stream of nitrogen. For MS analysis, samples were resuspended in 100 μ l chloroform:methanol:de-ionized water (73:23:3 v/v/v) to a concentration of 2 ng μ l⁻¹.

For MS analysis, lipids were separated on a Diol column (MultoHigh 100 Diol 5 μ HILIC Column, CS-Chromatographie Service GmbH) applying a 15 min linear gradient of mobile phase A (80% chloroform, 19.5% methanol and 0.5% ammonium hydroxide) and B (60.3% chloroform, 34.2% methanol, 5% de-ionized water and 0.5% ammonium hydroxide) from 0% B to 100% B. Conditions were kept at 100% B for the next 11 min, followed by a 5 min re-equilibration to 0% B. The injection volume was 2 μ l (4 μ g lipids). MS was performed with a Advion ExpressIon L, with scan mode 400–1,600 m/z , total scan time 50 min, scan speed 2,500 m/z -units/sec and scan time 240 ms.

Statistics and reproducibility. For Figs. 1, 2a, 4 and 6a,b and Extended Data Fig. 5a, the presented data are representative results from at least three independent experiments, unless otherwise specified in the figure legends. For Figs. 2b, 3 and 5 and Extended Data Figs. 1, 2, 3, 4 and 5b, quantifications were derived from three independent experiments or clones, unless specified otherwise in the figure legends. Whenever possible, individual data points of individual experiments are shown. GraphPad Prism 8, Windows Excel (version 2108) and Rstudio (1.4.1103) were used to analyse and plot data. No statistical method was used to pre-determine sample size. No data were excluded from analyses. The investigators were not blinded to allocation during the experiments or outcome assessment.

Reporting summary. Further information on research design is available in the Nature Research Reporting Summary linked to this article.

Data availability

MS data have been deposited to the MetaboLights metabolomics repository (dataset identifier MTBLS3415). Numerical source data (with all independent repeats) and unprocessed images of gels and blots are provided in the source data files. All other data supporting the findings of this study are available from the corresponding author on reasonable request. Source data are provided with this paper.

References

30. Janke, C. et al. A versatile toolbox for PCR-based tagging of yeast genes: new fluorescent proteins, more markers and promoter substitution cassettes. *Yeast* **21**, 947–962 (2004).
31. Longtine, M. S. et al. Additional modules for versatile and economical PCR-based gene deletion and modification in *Saccharomyces cerevisiae*. *Yeast* **14**, 953–961 (1998).
32. Helle, S. C. J. et al. Mechanical force induces mitochondrial fission. *eLife* **6**, e30292 (2017).
33. da Silveira Dos, S. A. X. et al. Systematic lipidomic analysis of yeast protein kinase and phosphatase mutants reveals novel insights into regulation of lipid homeostasis. *Mol. Biol. Cell* **25**, mbc.E14-03-0851 (2014).
34. Castro-Perez, J. M. et al. Comprehensive LC-MSE lipidomic analysis using a shotgun approach and its application to biomarker detection and identification in osteoarthritis patients. *J. Proteome Res.* **9**, 2377–2389 (2010).
35. Adams, K. J. et al. Skyline for small molecules: a unifying software package for quantitative metabolomics. *J. Proteome Res.* **19**, 1447–1458 (2020).
36. John Peter, A. T., Petrunger, C., Peter, M. & Kornmann, B. Monitoring ER–mitochondria lipid exchange *in vivo* using METALIC. Protocol Exchange <https://doi.org/10.21203/rs.3.pev-1882/v1> (2022).

Acknowledgements

We thank members of the Peter and Kornmann laboratories for insightful discussions and helpful suggestions. Microscopy analysis was carried out at the ETH Zürich ScopeM facility, and we thank T. Schwarz for outstanding technical support. Lipidomics measurements were performed at the Functional Genomics Center Zurich (FGCZ). We especially thank S. Streb and E. Laczko of the FGCZ Metabolomics division for establishing and optimizing lipidomics workflows, and for excellent technical guidance. Ylp204-pADH1-AtTIR1-9myc was a gift from H. Ulrich (Addgene plasmid #99532), and we are grateful to P. Kimmig for providing us the AtTIR1 construct in a pRS303

backbone. The Kornmann lab is supported by grants from the Swiss National Science Foundation (SNSF, 31003A_179549) and the Wellcome Trust (214291/A/18/Z). Work in the Peter laboratory was supported by the SNSF (310030_200426 / 1), the Synapsis Foundation (2020-PI03) and ETH Zürich. A.T.J.P. was supported by ETH Zürich/ Institute of Biochemistry, Spark grant of the SNSF (CRSK-3_190364) and a FreeNovation grant of the Novartis Foundation (TE-70768 FreeNovation), and C.P. by an EMBO fellowship (EMBO ALTF 298-2016).

Author contributions

A.T.J.P. and B.K. conceived the study. A.T.J.P. designed and performed all the experiments. C.P. designed and conducted the experiments related to expression of CFase in mammalian cells. M.P. and B.K. supervised the study. A.T.J.P. and B.K. analysed data and wrote the manuscript with input from C.P. and M.P.

Competing interests

The authors declare no competing interests.

Additional information

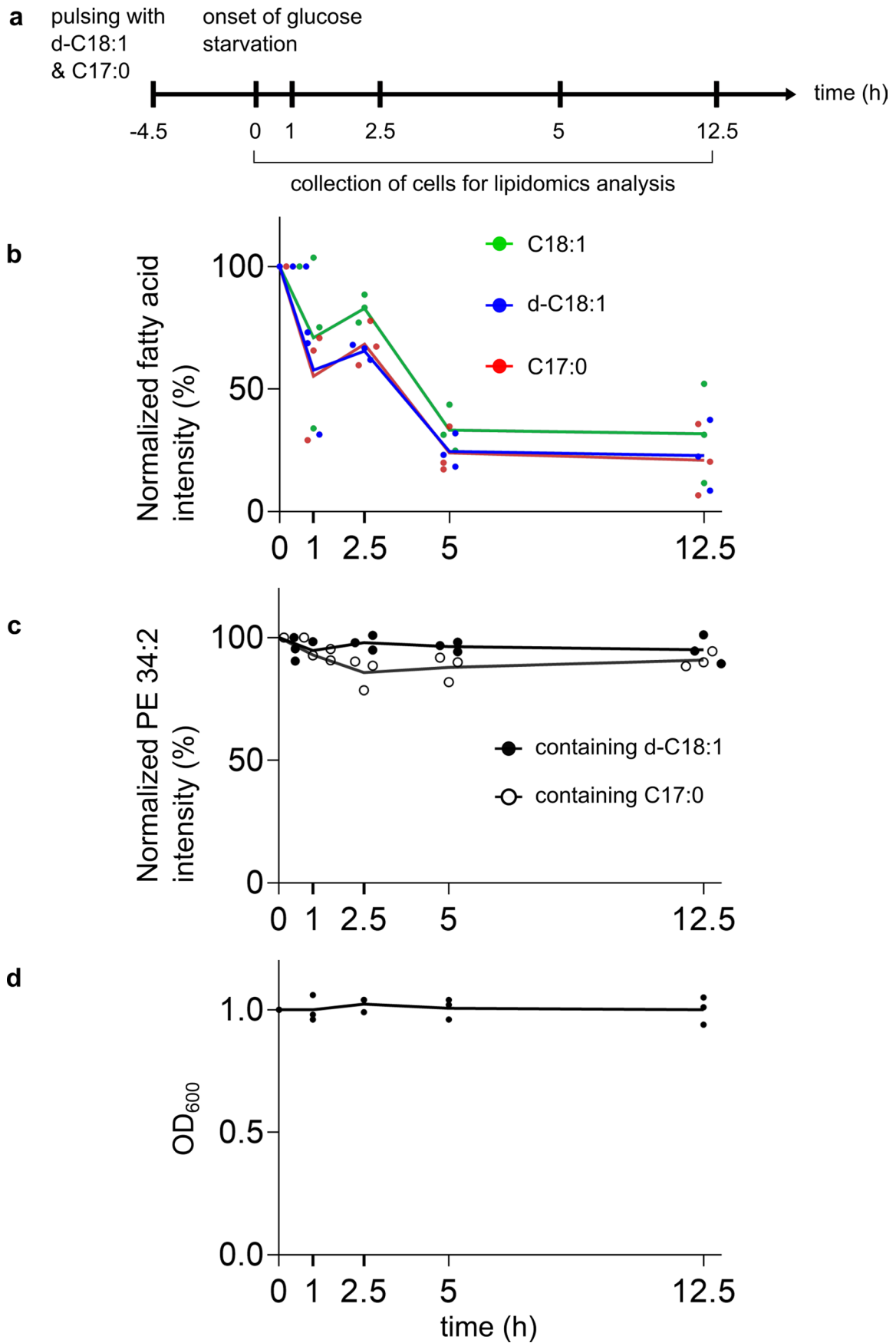
Extended data is available for this paper at <https://doi.org/10.1038/s41556-022-00917-9>.

Supplementary information The online version contains supplementary material available at <https://doi.org/10.1038/s41556-022-00917-9>.

Correspondence and requests for materials should be addressed to Arun T. John Peter or Benoît Kornmann.

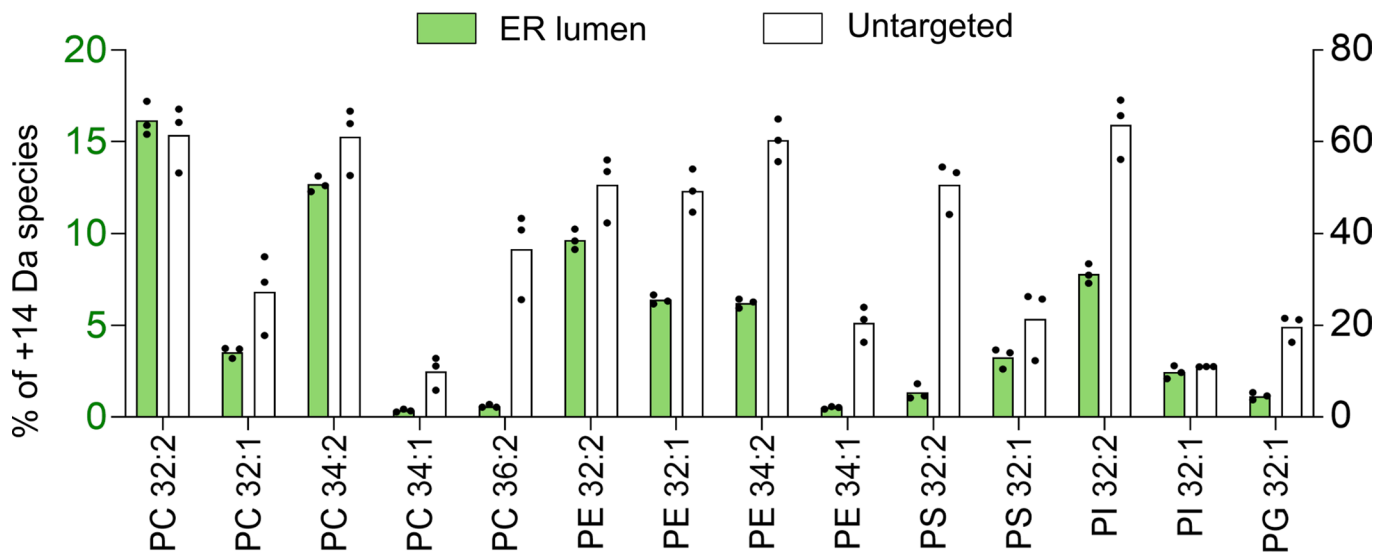
Peer review information *Nature Cell Biology* thanks W. Mike Henne, and the other, anonymous reviewer(s) for their contribution to the peer review of this work. Peer reviewer reports are available.

Reprints and permissions information is available at www.nature.com/reprints.

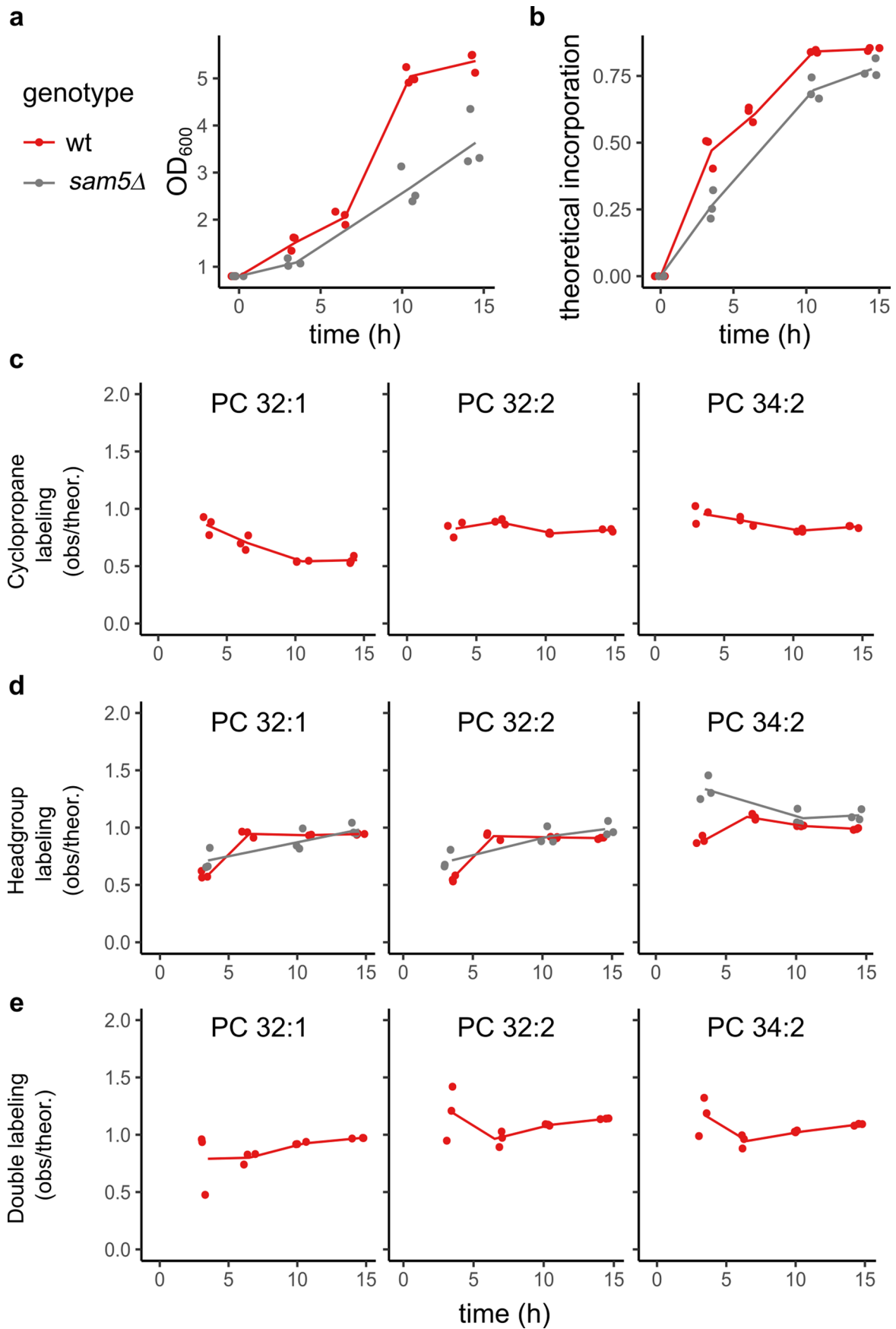


Extended Data Fig. 1 | See next page for caption.

Extended Data Fig. 1 | Cyclopropane fatty acid and its unsaturated counterpart are metabolized in a similar manner. **a**, Depiction of the time points at which wild-type cells were collected for lipidomics analysis upon onset of glucose starvation, post pulse-labeling with deuterated oleic acid d-C18:1 and cyclopropane fatty acid C17:0 for 4.5 hours. **b**, Line plot showing the intensity of the endogenous oleic acid (C18:1) and the ectopically provided deuterated oleic acid (d-C18:1) or cyclopropane fatty acid (C17:0) over time upon onset of glucose starvation. **c**, Line plot showing the intensity of a phosphatidylethanolamine (PE) species that has either incorporated d-C18:1 or C17:0 as one of its fatty acid moieties. **d**, The growth profile of pulse-labeled wild-type cells post glucose starvation. Source numerical data are available in source data.



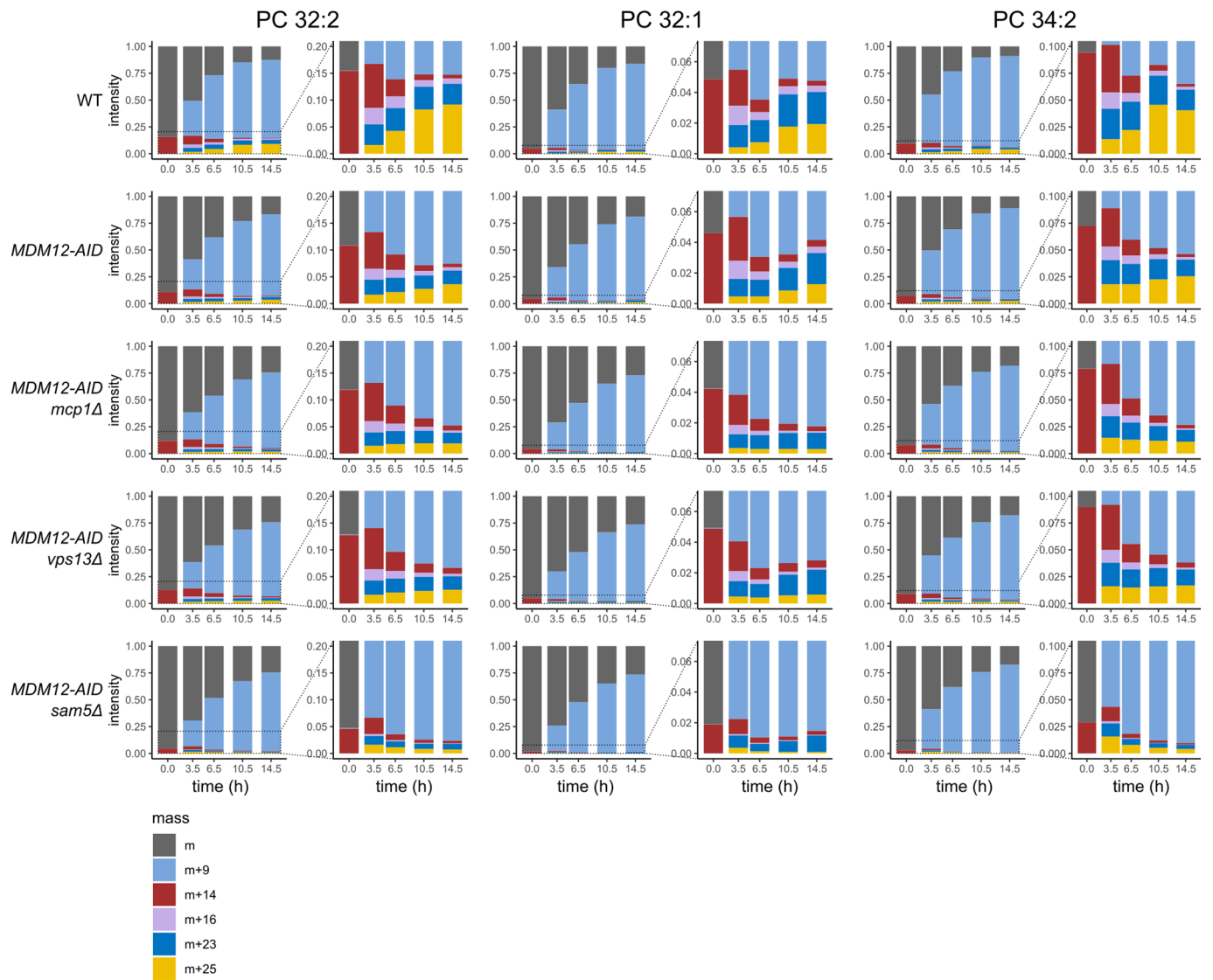
Extended Data Fig. 2 | CFAse targeted to the ER lumen has the different modification profile than its untargeted counterpart. Bar plot showing the percentage of each indicated phospholipid species that is mass-tagged upon constitutive expression of organelle-targeted CFAse in yeast. Values for the cytosolic (untargeted) CFAse are read on the right axis, values for the ER-lumen targeted CFAse are read on the left axis. Percentage values represent the mean derived from experiments done on three independent clones. Source numerical data are available in source data.



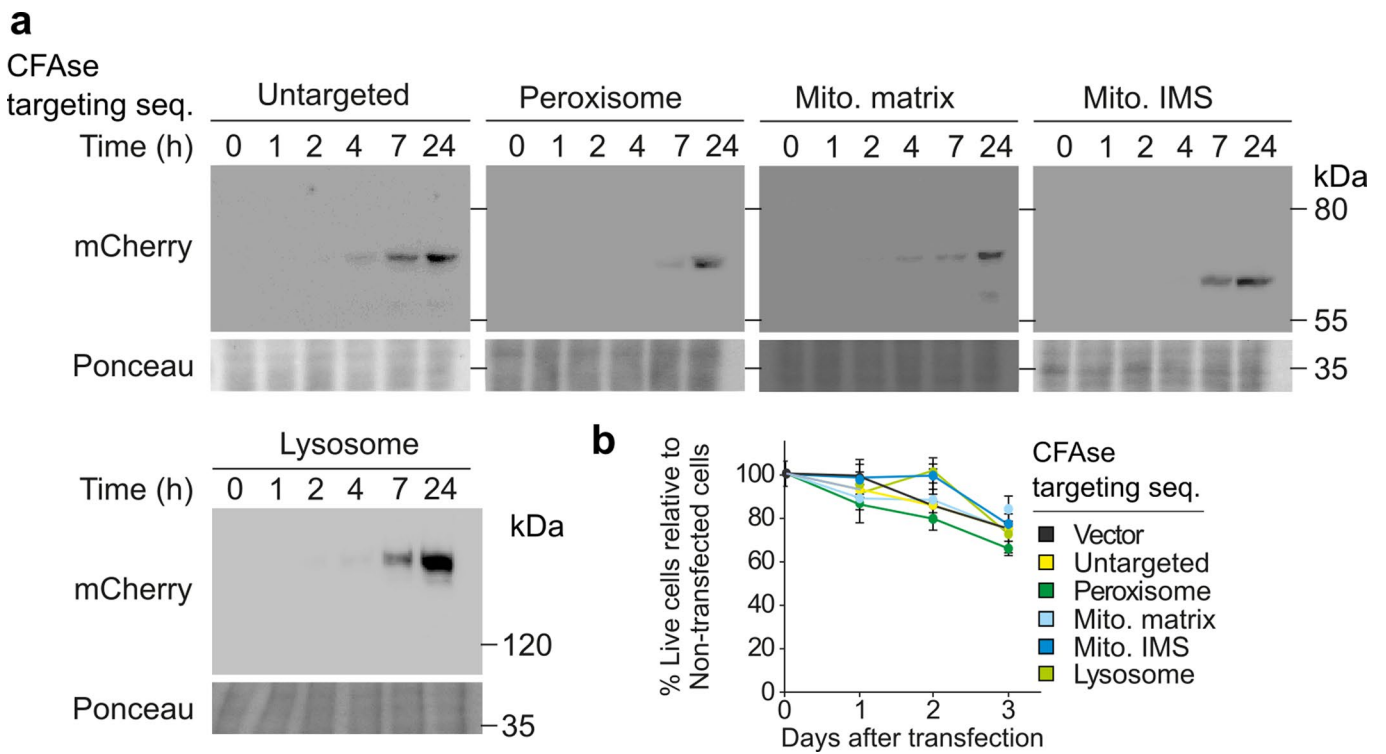
Extended Data Fig. 3 | See next page for caption.

Extended Data Fig. 3 | Theoretical deuterium incorporation. **a**, OD_{600} of the cultures used in Fig. 3 (Note that OD measurements are missing for the *sam5Δ* strains at $t_{6.5}$). **b**, Theoretical ratio of newly synthesized over total lipid expected if the abundance of newly synthesized lipids is proportional to the change of OD_{600} in the culture minus the starting OD_{600} , *i.e.*: Theoretical incorporation = $(OD_{600} - 0.8) / OD_{600}$. **c**, Ratio of the observed incorporation to the theoretical incorporation (as displayed in B) for CFAse activity, where CFA labeling is the sum of the +16 and +25 kDa species. **d**, Ratio of the observed incorporation (as displayed in Fig. 3c) to the theoretical incorporation (as displayed in B) for methyltransferase activity. **e**, Ratio of the observed double label incorporation (as displayed in Fig. 3) to the theoretical one calculated as the product of the headgroup and CFA labeling. Source numerical data are available in source data.

+ auxin



Extended Data Fig. 4 | Raw proportion of each lipid species. Normalized bar plot showing the relative changes in intensities of different labeled species with time (hours), from the onset of d-methionine labeling in auxin-treated cells. The changes are shown for three different phospholipid species, PC 32:2 (a), PC 32:1 (b) and PC 34:2 (c). Inset shows magnified views to better follow the intensity changes in species with a cyclopropane ring. Source numerical data are available in source data.



Extended Data Fig. 5 | CFase can be expressed inducibly and is not toxic in HeLa cells. **a**, Expression of mCherry-tagged CFase variants in HeLa cells after doxycycline induction (1 µg/ml) for one hour. Expression was monitored by western blot at the indicated time points. This experiment was performed once but similar results were obtained in Fig. 6. **b**, Cell viability upon CFase expression. CFase expression was induced by doxycycline (1 µg/ml) for the indicated time. The medium was replaced every 24 hours; Data represent the mean ± S.D from three independent experiments. Source numerical data and unprocessed blots are available in source data.

Reporting Summary

Nature Portfolio wishes to improve the reproducibility of the work that we publish. This form provides structure for consistency and transparency in reporting. For further information on Nature Portfolio policies, see our [Editorial Policies](#) and the [Editorial Policy Checklist](#).

Statistics

For all statistical analyses, confirm that the following items are present in the figure legend, table legend, main text, or Methods section.

- | | |
|-----|-----------|
| n/a | Confirmed |
|-----|-----------|
- The exact sample size (n) for each experimental group/condition, given as a discrete number and unit of measurement
 - A statement on whether measurements were taken from distinct samples or whether the same sample was measured repeatedly
 - The statistical test(s) used AND whether they are one- or two-sided
Only common tests should be described solely by name; describe more complex techniques in the Methods section.
 - A description of all covariates tested
 - A description of any assumptions or corrections, such as tests of normality and adjustment for multiple comparisons
 - A full description of the statistical parameters including central tendency (e.g. means) or other basic estimates (e.g. regression coefficient) AND variation (e.g. standard deviation) or associated estimates of uncertainty (e.g. confidence intervals)
 - For null hypothesis testing, the test statistic (e.g. F , t , r) with confidence intervals, effect sizes, degrees of freedom and P value noted
Give P values as exact values whenever suitable.
 - For Bayesian analysis, information on the choice of priors and Markov chain Monte Carlo settings
 - For hierarchical and complex designs, identification of the appropriate level for tests and full reporting of outcomes
 - Estimates of effect sizes (e.g. Cohen's d , Pearson's r), indicating how they were calculated

Our web collection on [statistics for biologists](#) contains articles on many of the points above.

Software and code

Policy information about [availability of computer code](#)

Data collection Growth curves were obtained using the Clariostar software (version 5.4). Western blots were imaged using FusionCapt Advance FX7 software (version 17.03). Microscopy images were obtained using the Deltavision softWoRx software (version 6.5.2). Mass spectrometry data were obtained using the Thermo Q.Exactive XCalibur software (version 4.0.27.10).

Data analysis Image processing for microscopy and western blots: FIJI (Image J 1.53c)
Statistics and Visualization: GraphPad Prism 8, Excel for Windows (Version 2108), RStudio (1.4.1103)
Lipidomics data analysis: Skyline software (version 21.2.0.369)

For manuscripts utilizing custom algorithms or software that are central to the research but not yet described in published literature, software must be made available to editors and reviewers. We strongly encourage code deposition in a community repository (e.g. GitHub). See the Nature Portfolio [guidelines for submitting code & software](#) for further information.

Data

Policy information about [availability of data](#)

All manuscripts must include a [data availability statement](#). This statement should provide the following information, where applicable:

- Accession codes, unique identifiers, or web links for publicly available datasets
- A description of any restrictions on data availability
- For clinical datasets or third party data, please ensure that the statement adheres to our [policy](#)

Mass spectrometry data have been deposited to the MetaboLights metabolomics repository (dataset identifier MTBLS3415). Numerical source data (with all independent repeats) and unprocessed images of gels and blots are provided in the Source Data files. All other data supporting the findings of this study are available from the corresponding author on reasonable request. Source data are provided with this paper.

Field-specific reporting

Please select the one below that is the best fit for your research. If you are not sure, read the appropriate sections before making your selection.

- Life sciences Behavioural & social sciences Ecological, evolutionary & environmental sciences

For a reference copy of the document with all sections, see [nature.com/documents/nr-reporting-summary-flat.pdf](https://www.nature.com/documents/nr-reporting-summary-flat.pdf)

Life sciences study design

All studies must disclose on these points even when the disclosure is negative.

Sample size	Experiments were performed a minimum of three times as a standard in the field.
Data exclusions	No data was excluded in this study
Replication	All data result from three independent experiments or experiments performed on three independent clones, unless otherwise stated with similar results. The number of replicates for each experiment is stated in the figure legends.
Randomization	For mass spectrometry runs, samples were randomized before queueing them in the autosampler. No other randomization was done, as the samples were derived from genetically identical, single colonies, and processed at the same time.
Blinding	No blinding was performed. All quantifications were performed without human interference.

Reporting for specific materials, systems and methods

We require information from authors about some types of materials, experimental systems and methods used in many studies. Here, indicate whether each material, system or method listed is relevant to your study. If you are not sure if a list item applies to your research, read the appropriate section before selecting a response.

Materials & experimental systems

n/a	Involved in the study
<input type="checkbox"/>	<input checked="" type="checkbox"/> Antibodies
<input type="checkbox"/>	<input checked="" type="checkbox"/> Eukaryotic cell lines
<input checked="" type="checkbox"/>	<input type="checkbox"/> Palaeontology and archaeology
<input checked="" type="checkbox"/>	<input type="checkbox"/> Animals and other organisms
<input checked="" type="checkbox"/>	<input type="checkbox"/> Human research participants
<input checked="" type="checkbox"/>	<input type="checkbox"/> Clinical data
<input checked="" type="checkbox"/>	<input type="checkbox"/> Dual use research of concern

Methods

n/a	Involved in the study
<input checked="" type="checkbox"/>	<input type="checkbox"/> ChIP-seq
<input checked="" type="checkbox"/>	<input type="checkbox"/> Flow cytometry
<input checked="" type="checkbox"/>	<input type="checkbox"/> MRI-based neuroimaging

Antibodies

Antibodies used	<i>mouse anti-Pgk1 antibody (Invitrogen, 459250, 1:3000 dilution), rat anti-RFP antibody (Chromotek, 5F8, 1:1000 dilution), mouse anti-FLAG antibody (Sigma, F1804, 1:1000), rabbit anti-mCherry antibody, ab167453, 1:1000) and horseradish peroxidase-coupled secondary antibody (Bio-Rad, 170-6516; 1:10,000 dilution)</i>
Validation	<i>Antibodies were purchased from Invitrogen, Chromotek, Sigma, Abcam and have been validated in previous publications or by the manufacturer. mCherry antibody was validated using cell extract from HEK293 cells transfected with pFin-EF1-mCherry vector. For Pgk1, see https://doi.org/10.1038/s41556-021-00760-4; for RFP antibody, see https://doi.org/10.1089/hyb.2007.0555 and for FLAG antibody, see https://doi.org/10.1093/nar/gkab511</i>

Eukaryotic cell lines

Policy information about [cell lines](#)

Cell line source(s)	<i>HeLa cells were obtained from ATCC.</i>
Authentication	<i>HeLa cell line used in this study was not authenticated</i>
Mycoplasma contamination	<i>The cell lines were routinely tested for mycoplasma contamination and the results were negative.</i>
Commonly misidentified lines (See ICLAC register)	<i>HeLa cell line used in this study is not listed in the ICLAC database</i>